BIOCHEMISTRY
including biophysical chemistry & molecular biology

Article

pubs.acs.org/biochemistry

The Cellular Environment Stabilizes Adenine Riboswitch RNA Structure

Jillian Tyrrell,[†] Jennifer L. McGinnis,[†] Kevin M. Weeks,*[,†] and Gary J. Pielak*[,†,‡,§]

[†]Department of Chemistry, [‡]Department of Biochemistry and Biophysics, and [§]Lineberger Comprehensive Cancer Center, University of North Carolina at Chapel Hill, Chapel Hill, North Carolina 27599-3290, United States

Supporting Information

ABSTRACT: There are large differences between the intracellular environment and the conditions widely used to study RNA structure and function *in vitro*. To assess the effects of the crowded cellular environment on RNA, we examined the structure and ligand binding function of the adenine riboswitch aptamer domain in healthy, growing *Escherichia coli* cells at single-nucleotide resolution on the minute time scale using SHAPE (selective 2′-hydroxyl acylation analyzed by primer extension). The ligand-bound aptamer structure is essentially the same in cells and in buffer at 1 mM Mg^{2+}, the approximate Mg^{2+} concentration we measured in cells. In contrast, the in-cell conformation of the ligand-free aptamer is much more similar to the fully folded ligand-bound state. Even adding high Mg^{2+} concentrations to the buffer used for *in vitro* analyses did not yield the conformation observed for the free aptamer in cells. The cellular environment thus stabilizes the aptamer significantly more than does Mg^{2+} alone. Our results show that the intracellular environment has a large effect on RNA structure that ultimately favors highly organized conformations.

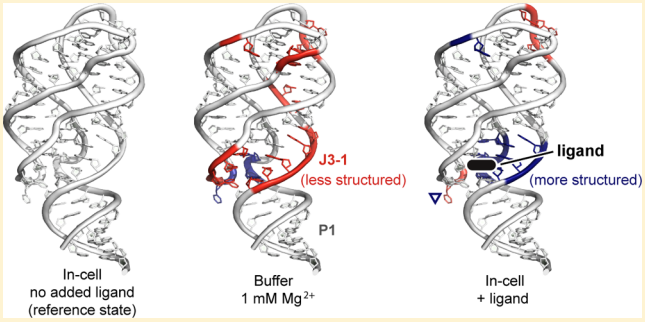

The intracellular environment is vastly different from the simple buffered solutions used in most *in vitro* explorations of biological macromolecular structure and function. For example, macromolecules reach concentrations of 300 g/L and occupy up to 30% of the total cellular volume,[1] and cells contain complex mixtures of metabolites, ions, and polyamines.[2−4] The highly crowded intracellular environment increases the importance of two types of interactions between macromolecules: hard-core repulsions and chemical interactions.[5] Hard-core repulsions reflect the impenetrable nature of atoms. These interactions reduce the available conformational space, thus favoring compact states.[6,7] Chemical interactions can be attractive or repulsive. Repulsions arise from contacts between like charges and reinforce the stabilizing hard-core effect. Attractive interactions include hydrogen bonding, juxtaposed complementary charges, hydrophobic contacts, and binding by numerous cellular proteins. Attractive interactions that expose more interacting surface to the crowding molecules destabilize folded, compact states,[8,9] whereas specific protein binding will be stabilizing. Low-molecular weight species in the cytoplasm, including metabolites, polyamines, and magnesium ion, also impose a combination of hard-core repulsions, nonspecific chemical interactions, and direct binding that are difficult to recapitulate *in vitro*.

RNA molecules are responsible for diverse cellular functions, many governed by precise features of their three-dimensional structures. *In vitro* studies show that crowding by synthetic polymers has dramatic consequences on RNA folding.[10−12] In addition, the negatively charged backbone of RNA makes folding highly sensitive to cation and polyamine concentrations.[13,14] Despite these considerations, most explorations of RNA structure and function employ purified RNAs and simple buffered solutions at Mg^{2+} concentrations significantly higher than those in cells. Studies of RNA structure *in vitro* have yielded many important insights into the roles of structural motifs in RNA function; however, a critical goal is to quantitatively monitor and understand the structure of RNA and its interactions with small molecule and protein ligands in the cellular environment.

The most widely used approach for probing RNA structure in cells has employed the reagent dimethyl sulfate (DMS), and these studies have yielded new information about the intracellular structure of several RNAs.[15,16] However, DMS reacts with only a few functional groups, primarily with adenosine (N1), to a lesser extent with cytosine (N3), and with guanosine (N7, although this latter adduct is not generally assayed in *in vivo* studies). *In vivo* DMS probing studies are therefore best coupled with other information.[16]

Here, we apply SHAPE (selective 2′-hydroxyl acylation analyzed by primer extension) using the fast-acting 1M7 reagent, which reacts nearly equally with all four RNA nucleotides,[17] to probe the effect of the intracellular environ-

Received: August 30, 2013
Revised: November 5, 2013
Published: November 11, 2013

   dx.doi.org/10.1021/bi401207q | *Biochemistry* 2013, 52, 8777−8785

ment on RNA structure. SHAPE yields quantitative information about the degree to which a nucleotide is constrained by base pairing or other interactions and has been widely used to develop secondary structure models and to detect complex conformational changes in RNA *in vitro*,[18−22] within membrane-encapsulated viruses,[23,24] and in cells.[25] Applying SHAPE chemistry to living cells promises to improve our understanding of how the intracellular environment affects RNA structure.

Riboswitch RNAs regulate gene expression by undergoing ligand-induced conformational changes that ultimately enhance or inhibit expression of a linked gene.[26] The *add* adenine riboswitch structure has been well characterized *in vitro*. Its function *in vivo* depends on binding the small metabolite adenine with high specificity. In the absence of ligand, the aptamer domain has a disordered binding pocket; when the ligand binds, stable tertiary interactions form (Figure 1A).[26−31]

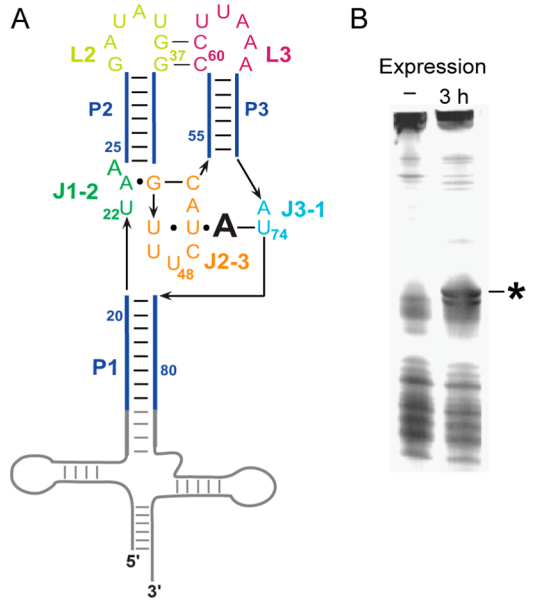

Figure 1. Expression of the adenine aptamer domain in *E. coli*. (A) Structure of the aptamer−tRNA construct. The adenine ligand is shown as a large A. The numbering corresponds to that of the *add* aptamer domain.[32] (B) Total cellular RNA 3 h after the induction of aptamer expression, visualized by denaturing polyacrylamide gel electrophoresis. The 143-nucleotide aptamer−tRNA chimera product is marked with an asterisk.

We probed the ligand-bound and ligand-free states of the adenine riboswitch aptamer domain in live *Escherichia coli* cells. Although many nonspecific RNA interactions occur in cells, ligand binding to the aptamer is highly specific and causes large and well-defined changes in SHAPE reactivity. The conformations of the ligand-bound aptamer in cells and in buffer were highly similar; in strong contrast, the ligand-free form was generally less reactive in cells than in buffer. Moreover, the pattern of SHAPE reactivity in cells could not be achieved in buffers containing 30 times the intracellular Mg^{2+} concentration. The results show that the net effect of the intracellular environment is to stabilize RNA tertiary structure and emphasize the importance of studying and understanding RNA structure in cells.

EXPERIMENTAL PROCEDURES

Concentration of Mg^{2+} in *E. coli* Cells. Free Mg^{2+} was measured using the intracellular chelator, mag-fura-2, acetoxymethyl (AM). The free Mg^{2+} concentration was obtained from the ratio of the fluorescence intensities of the free and complexed dyes at 510 nm measured using excitation 380 and 340 nm, respectively. Methods were adapted from those described previously.[33] *E. coli* BL21(DE3) cells were grown in Luria-Bertani (LB) medium at 37 °C, while being shaken, until the optical density at 600 nm (OD_{600}) reached ∼1. Aliquots (12 mL) were centrifuged at room temperature for 15 min at 1500*g*, washed once, and resuspended in 1.5 mL of Mg^{2+}-free buffer {10 mM 2-[4-(2-hydroxyethyl)piperazin-1-yl]-ethanesulfonic acid (HEPES) (pH 7.4), 200 mM potassium acetate, and 5 mM NaCl}. Cells were shaken at 37 °C for 10 min, and then 500 μL of the dye mixture containing 20 μM mag-fura-2 AM and 60 μM Pluronic F-127 (Molecular Probes) was added. Dyes were prepared in Mg^{2+}-free buffer from mag-fura-2 AM (5 mM, in anhydrous DMSO) and Pluronic F-127 [20% (w/v) in DMSO] stocks. After dye had been added, cells were shaken for 70 min at 37 °C. Cells were then washed, resuspended in 2 mL of Mg^{2+}-free buffer, and incubated for 30 min to ensure hydrolysis of the intracellular dye. Cells were then washed twice and resuspended in Mg^{2+}-free buffer to yield an OD_{600} of ∼0.5 (∼2 × 10^8 cells/mL). Cell viability was determined by plating serial dilutions of cell suspensions on LB-agar plates containing 1 mg/mL ampicillin.

The fluorescence of cell suspensions (2.4 mL in a 3 mL stirred cuvette) was measured at 37 °C using a Varian Cary Eclipse fluorimeter. Excitation at 340 and 380 nm was alternated at 1 s intervals, and emission was measured at 510 nm. To quantify Mg^{2+}-dependent changes in fluorescence, Mg^{2+} was added to cells at 100 s intervals (Figure S1A of the Supporting Information). The intensities and 340 nm/380 nm ratios were used to calculate the internal Mg^{2+} concentration:[34]

$$[Mg^{2+}] = K_D(F_0/F_S)(R - R_{min})/(R_{max} - R) \quad (1)$$

where K_D is the dissociation constant of the mag-fura-2−Mg^{2+} complex [2.5 mM (see below)], F_0/F_S is the ratio of intensities with 380 nm excitation for no added Mg^{2+} to saturating Mg^{2+}, R is the ratio of 510 nm emission from excitation at 340 and 380 nm at a given external Mg^{2+} concentration, and R_{min} and R_{max} are the minimal and maximal ratios determined at 0 mM Mg^{2+} and a saturating Mg^{2+} concentration, respectively. R_{min} and R_{max} were obtained at the end of each experiment by adding Mg^{2+} to a final concentration of 30 mM and then adding SDS [to a final concentration of 0.1% (w/v)] to lyse the cells; lysis causes mag-fura-2 to be released from cells and to be saturated with extracellular Mg^{2+} (Figure S1B of the Supporting Information). This step was followed by addition of EDTA to a final concentration of 60 mM to chelate Mg^{2+} and achieve a free Mg^{2+} measurement. The K_D was determined by recording Mg^{2+}-dependent fluorescence changes for hydrolyzed mag-fura-2 (0.4 μM) in buffer and fitting the 510 nm intensities from 340 nm excitation to a one-site binding curve (Figure S2 of the Supporting Information). Emission from cells in Mg^{2+}-free buffer was constant over time (Figure S1A of the Supporting Information). Intensities were corrected for autofluorescence, which was also constant and lower than that of dye-loaded cells by a factor of 13 for excitation at 340 nm and a factor of 20 for excitation at 380 nm (inset of Figure S1B of the Supporting

dx.doi.org/10.1021/bi401207q | *Biochemistry* 2013, 52, 8777−8785

Information). Serial dilution and plating of cells confirmed that ~90% of the dye-loaded cells were viable.

Vector Construction. The sequence encoding the adenine riboswitch aptamer domain was inserted between the TΨC and D stem-loops of human $tRNA^{lys3}$ as a synthetic gene in a pIDTSMART vector (IDT) (Figure S3 of the Supporting Information). The gene was inserted into pET21a(+) using *Hin*dIII (5′) and *Xba*I (3′) cloning sites for expression under the control of a T7 promoter (Figure S3 of the Supporting Information). The transcript is a chimeric tRNA in which the anticodon stem is replaced with the adenine riboswitch aptamer domain.[35,36]

RNA Expression. The aptamer−tRNA construct (Figure 1B) was expressed in *E. coli* BL21(DE3) cells in LB medium at 37 °C. When the OD_{600} reached 0.6, RNA expression was induced by addition of isopropyl β-D-1-thiogalactopyranoside (1 mM). Expression was allowed to proceed for 30 min, at which time aliquots were removed and added to 2-aminopurine, 2,6-diaminopurine, or 3-methyladenine dissolved in LB (final concentration of 1 mM) or to LB medium alone. Expression was continued for 1 h, at which time cell aliquots were subjected to either in-cell or *in vitro* SHAPE.

In-Cell SHAPE. The aptamer construct was expressed in the presence or absence of ligand as described above. Following RNA expression, cellular RNA was modified by adding aliquots of cells (1 mL) to 20 μL of 300 mM 1M7 in DMSO or to neat DMSO [final cosolvent concentration of 2% (v/v)]. The samples were incubated while being shaken for 3 min at 37 °C. Total cellular RNA was recovered from protoplasts and isolated as described previously.[37] RNA was precipitated with ethanol, washed three times with 70% (v/v) aqueous ethanol, and resuspended in 15 μL of deionized H_2O. Primer extension of the aptamer construct was achieved using sequence-specific primers, containing locked nucleic acid (LNA) nucleotides, and 5′ fluorescent labels as outlined below. cDNA products were resolved by capillary electrophoresis.

To measure the concentration of the aptamer construct in the cellular RNA, aliquots of total RNA and serial dilutions of the purified construct were analyzed by denaturing polyacrylamide gel electrophoresis. Gels were stained with SYBR Gold (Invitrogen), and a standard curve was constructed using the band intensities of samples corresponding to the purified construct. The standard curve was used to determine the concentration of the aptamer construct in the total RNA samples. The aptamer construct (~7 g/L) was ~7% of the total RNA concentration (100 g/L, determined by UV spectroscopy). We estimated the concentration of the aptamer construct in cells to be 7% of the total RNA in *E. coli* (75−120 g/L[38]). From the molecular mass of the construct (43.4 kDa), the concentration of the construct in cells is 120−190 μM.

***In Vitro* SHAPE.** Following expression, RNA was recovered from protoplasts and isolated as described previously[37] and incubated in 50 mM HEPES (pH 8.0), 200 mM potassium acetate (pH 8.0), and 1−30 mM $MgCl_2$ for 30 min. The aptamer construct was purified by anion exchange, fast performance liquid chromatography. Ligand (1 mM) was added after folding, and incubation was continued for 10 min. The aptamer construct (8 pmol) was then added to 1/50 volume of 300 mM 1M7 in DMSO or to neat DMSO. The samples were incubated at 37 °C for 3 min. RNA was precipitated with ethanol, washed three times with 70% (v/v) aqueous ethanol, and resuspended in 15 μL of deionized H_2O.[37] Primer extension and capillary electrophoresis were then used to determine the sites of adduct formation.

Primer Extension. A 12-nucleotide DNA primer (Exiqon) complementary to the 5′ end of the acceptor stem and containing three locked nucleic acid (LNA) nucleotides (5′-*T*GGCGCCCGAAC-3′, where italic font indicates LNA nucleotides) was used. The primer was labeled with either a 5′ 6-FAM or 5-HEX fluorescent dye. The 6-FAM-labeled primer was used for the (+) or (−) 1M7 channels; the 5-HEX-labeled primer was used for the sequencing channel. The RNA (1.5 μg) and primer (2 pmol) were mixed and diluted to 13 μL with H_2O. The sample was then incubated for 5 min at 65 °C and then on ice for 3 min. The reaction mixture contained 4 μL of 5× SuperScript first-strand buffer, 1 μL of 0.1 M dithiothreitol, 1 μL of dNTPs (10 mM each), and 1 unit of SuperScript III (Invitrogen). For sequence analysis, the reaction mixtures were prepared as described above, except the RNA was not treated with 1M7 or DMSO, the RNA/primer mixture was diluted to 12 μL, and 1 μL of 10 mM ddATP was added prior to adding SuperScript III. Reaction mixtures were incubated at 55 °C for 60 min and then at 70 °C for 15 min. cDNA was recovered by ethanol precipitation and washed three times with 70% (v/v) aqueous ethanol. Pellets were dried under vacuum and resuspended in 10 μL of deionized formamide. The products were resolved by capillary electrophoresis on an Applied Biosystems 3500 DNA capillary electrophoresis instrument.

SHAPE Data Analysis. Electropherograms were analyzed with QuShape.[39] After baseline and mobility shift corrections, peaks in the (+) and (−) 1M7 channels were aligned, and Gaussian integration was used to quantify peak areas. The SHAPE reactivity is reported as the area of the (+) 1M7 peaks minus the area of the no-reagent background peaks. The absolute amount of adduct formed *in vitro* and in cells was calculated on the basis of the probabilities of termination of primer extension, as described.[39]

RESULTS

Intracellular Mg^{2+} Concentration. RNA tertiary structure depends on Mg^{2+} concentration.[13,31] We measured the free Mg^{2+} concentration in *E. coli* cells using a ratiometric Mg^{2+}-selective fluorophore (Figure 2 and Figures S1 and S2 of the Supporting Information)[34] to ensure that relevant concen-

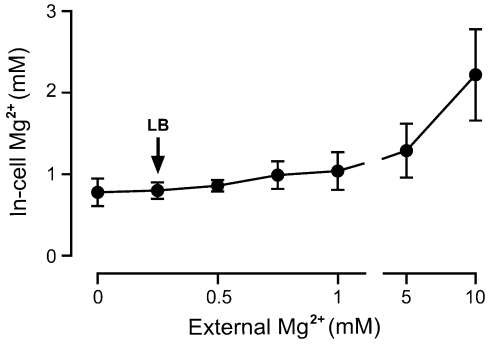

Figure 2. Free Mg^{2+} concentration in *E. coli* cells measured using the ion-selective fluorophore, mag-fura-2. The free concentration in cells at the late-log phase is 0.8 ± 0.2 mM in standard LB medium at 37 °C (arrow). The external concentration in standard LB medium is 0.25 mM. Error bars show the standard deviation of the mean from three trials.

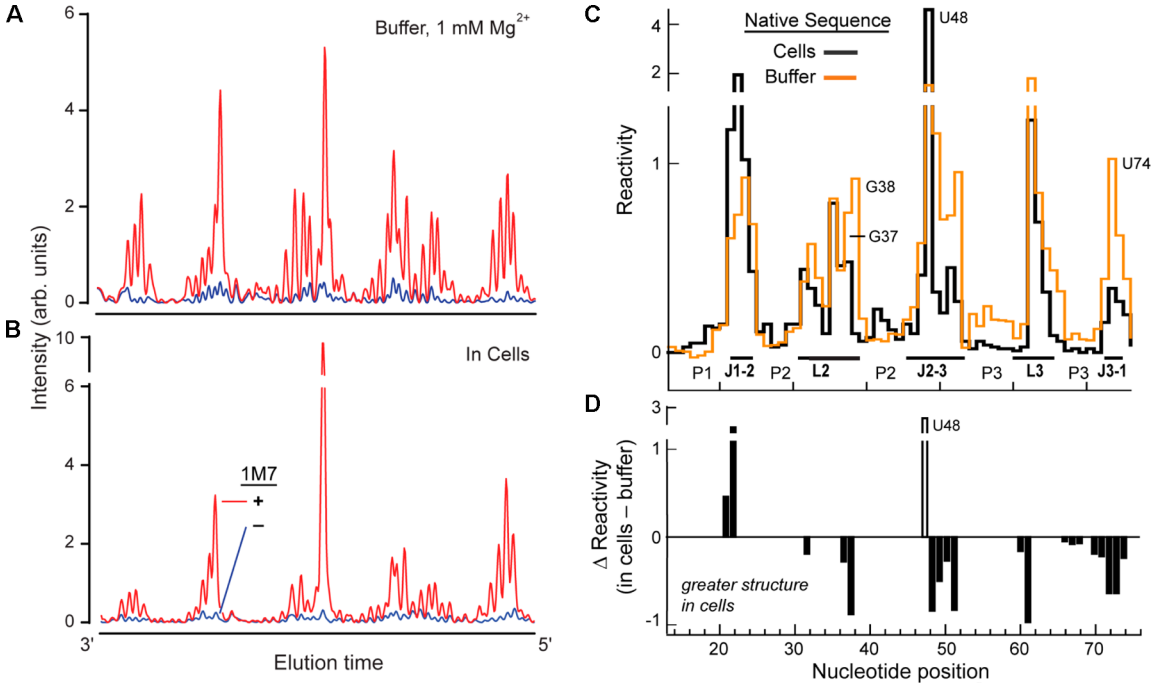

Figure 3. In-cell SHAPE. Electropherograms showing SHAPE reactivity profiles for the native sequence adenine aptamer domain obtained (A) in buffer at a near-physiological Mg^{2+} (1 mM) and (B) in cells. (C) Processed SHAPE reactivity profiles for the adenine aptamer domain in cells (black) and in buffer at 1 mM Mg^{2+} (orange). (D) Difference plot of SHAPE reactivities in cells compared to buffer. Only statistically significant differences are shown (two-tailed Student's *t* test; $p < 0.02$; $n = 3$). The open bar indicates that U48 is constrained in a rare hyper-reactive conformation (Figure S7 of the Supporting Information); thus, a positive difference at this position reflects a higher level of structure in cells.

trations were used for *in vitro* experiments. Cells were grown to the late-log phase, and the intracellular Mg^{2+} concentration was quantified as a function of external Mg^{2+} concentration. At an external concentration corresponding to that in LB medium (0.3 mM, calculated from the Mg^{2+} content of Tryptone and yeast extract[40]), the intracellular Mg^{2+} concentration was 0.8 ± 0.2 mM (Figure 2, arrow). The intracellular free Mg^{2+} concentration increased only slightly with an increase in the extracellular concentration; the concentration did not increase above 1 mM until the extracellular concentration was 5 mM and reached 2.2 ± 0.5 mM at an external concentration of 10 mM (Figure 2). Our measurement of the free Mg^{2+} concentration in *E. coli* cells (0.8 ± 0.2 mM) is consistent with measurements of free Mg^{2+} concentrations in other cell types.[33,41−43]

In-Cell SHAPE. To study the aptamer domain in *E. coli* cells, we expressed the RNA as a chimera in which the aptamer domain was inserted into the anticodon loop of $tRNA^{lys}$ (Figure 1A and Figure S3 of the Supporting Information). These chimeric RNAs fold stably in cells and are processed by nucleases that cleave tRNAs to yield an intact and monodisperse product.[35,36] The RNA containing the aptamer was processed into a product of approximately 143 nucleotides (Figure 1B).

In-cell SHAPE probing was achieved by adding 1-methyl-7-nitroisatoic anhydride (1M7)[44] in dimethyl sulfoxide (DMSO) to late log-phase cells, under conditions compatible with normal cell growth and viability (Figure S4 of the Supporting Information). 1M7 has a half-life of 24 s under conditions corresponding to those in culture medium in the late-log phase [37 °C and pH 7.0 (Figure S5 of the Supporting Information)]. A wide variety of experiments, spanning roughly 30 years of experimental work, suggest that small, slightly hydrophobic molecules penetrate cellular membranes and diffuse over the dimensions of an *E. coli* bacterium on a time scale of roughly 30−100 ms.[23,24,45−49] Thus, the half-life of 1M7 is roughly 1000 times longer than the time required to diffuse the length of an *E. coli* cell. In-cell RNA probing with 1M7 yields structural snapshots on the minute time scale.

We have consistently found that 1M7 is straightforward to use in cells, including bacterial cells. Reagents like 1M7 that react rapidly with RNA and reagents that react slowly[25] probe different structural features. In general, reagents that react on the minute time scale provide quantitative measurements of intrinsic RNA structure,[50−52] whereas slower reagents are sensitive to additional slower dynamic features of RNA, some of which vary with the ion environment. One consequence of this difference is that slow reagents are highly sensitive to *in vitro* ion concentrations,[44] whereas fast reagents are not. Thus, fast-reacting reagents like 1M7 are strongly preferred in making direct comparisons of in-cell and *in vitro* measurements without the need for corrections based on ion sensitivity.

After modification with 1M7, total cellular RNA was isolated, and sites of aptamer modification were detected by primer extension analyzed by capillary electrophoresis.[37] In-cell SHAPE probing with 1M7 yielded electropherograms comparable to or better in quality than those obtained from *in vitro* experiments (Figure 3A,B). SHAPE reactivities were highly reproducible for both *in vitro* and in-cell experiments (Figure S6 of the Supporting Information). Little or no degradation of the adenine riboswitch RNA was observed in the cells or *in vitro* upon treatment with DMSO. We also calculated the absolute amount of adduct formed for the free RNA, both in dilute solution and in cells, by integrating all observed peaks and calculating the amount of unmodified, full-length product.[39] The numbers of adducts per RNA were identical, 0.60 and 0.61,

dx.doi.org/10.1021/bi401207q | *Biochemistry* 2013, 52, 8777−8785

respectively. This corresponds to one modification every ~105 nucleotides both *in vitro* and in cells, or roughly one adduct per RNA. Thus, signals reflected the reactivity of the RNA with 1M7, and as expected,[23,24,45−49] the 1M7 reagent readily diffuses across the double-walled membrane of the Gram-negative *E. coli* bacterium.

In the in-cell reactivity profile for the aptamer in the absence of added ligand (Figure 3C and Figure S6 of the Supporting Information), nucleotides expected to form helices P1−P3 (Figure 1A) had low reactivity, consistent with stable base pairing in these structures. Most nucleotides that form the ligand binding pocket (J1-2, J2-3, and J3-1) were moderately (≥0.4) or highly (>0.8) reactive as were nucleotides in loop regions L2 and L3. Nucleotide U48 was hyper-reactive. The in-cell SHAPE reactivity profile for the free aptamer suggests the three major RNA helices are formed and that the ligand-binding pocket is flexible and partially disordered.

The Ligand-Free RNA Is More Highly Organized in Cells Than in Buffered Solution. We observed large differences between the structure of the unliganded aptamer in cells and its structure in buffer at 1 mM Mg^{2+} (Figure 3C). We subtracted the two SHAPE profiles from each other and identified statistically significant nucleotide reactivity differences (two-tailed Student's *t* test; $p < 0.02$; $n = 3$) (Figure 3D). Nucleotides G37 and G38 in L2 and C61 and C62 in L3 were significantly more reactive *in vitro* than in cells, suggesting that tertiary interactions involving loops L2 and L3[31,32] were largely absent in buffered solution but were at least partially formed in cells.

Most nucleotides in the adenine binding pocket (regions J2-3 and J3-1) were also less reactive in cells than *in vitro*, consistent with the formation of stacking and base pairing interactions in these regions in cells and the lack of these interactions in buffer. The major exceptions were two nucleotides in J1-2, which were more reactive in cells than in buffered solution. This higher reactivity may arise from increased solvent accessibility due to tertiary collapse and ordering of J2-3 and J3-1 or to attractive chemical interactions with other cellular components. Nucleotide U48 was hyper-reactive in cells but only highly reactive in buffer. In the crystal structure of the ligand-bound RNA, U48 is flipped into the solvent[32] and constrained in one of the rare conformations that activates the ribose 2′-hydroxyl group for SHAPE chemistry (Figure S7 of the Supporting Information).[53] Thus, hyper-reactivity at U48 is also indicative of a more highly structured RNA in cells.

Overall, as judged by nucleotide reactivities that report the L2−L3 tertiary interaction and the organization of the ligand-binding pocket, the aptamer features more nucleotides whose conformations are similar to that of the fully folded ligand bound state, suggesting it is more structured and has a more highly organized binding pocket in cells than in buffer at a physiological Mg^{2+} concentration.

Ligand Binding in Cells. The *add* riboswitch recognizes 2-aminopurine (2AP) (Figure 4A) and adenine with similar affinities (K_D values of ~117 and 60 nM, respectively[27,54,55]), and both ligands induce large conformational changes in the riboswitch RNA.[26,54,55] 2AP, however, is not found in detectable quantities in *E. coli*, and the expression level of our RNA construct is ~100 times the intracellular concentration of adenine (~10^{-6} M).[4] Thus, using 2AP, it is possible to examine the in-cell consequences of ligand binding without interference by endogenous cellular metabolites.

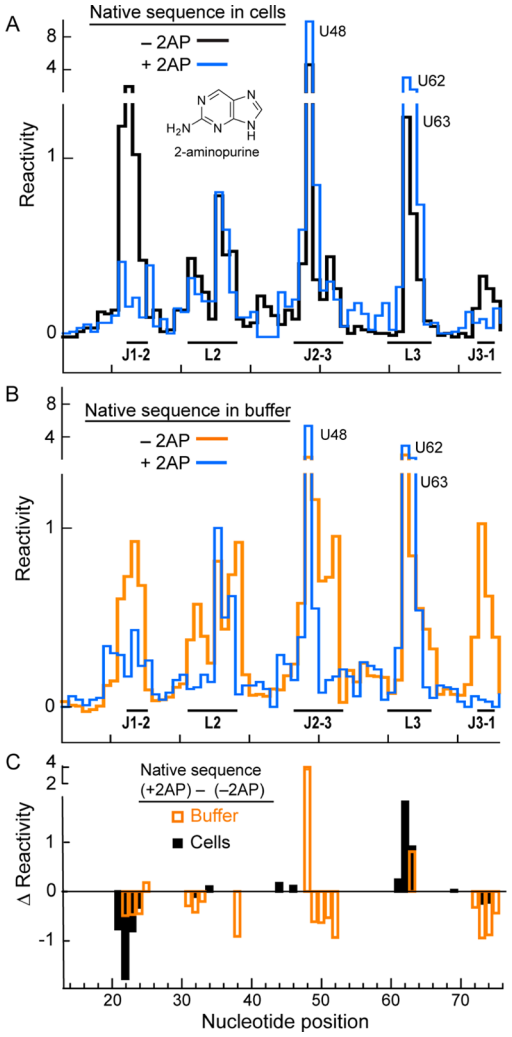

Figure 4. Ligand binding by the native sequence adenine aptamer in (A) cells and (B) buffer. When the ligand 2AP was present, its concentration was 1 mM. (C) Difference plot showing nucleotides with significant changes (two-tailed Student's *t* test; $p < 0.02$; $n = 3$) in reactivity upon ligand binding in cells (black) and buffer (orange).

We observed numerous changes in SHAPE reactivity for the aptamer expressed in *E. coli* when 2AP was added to the growth medium (Figure 4A). Significant differences (two-tailed Student's *t* test; $p < 0.02$; $n = 3$) are consistent with ligand-mediated conformational changes in the RNA and formation of the intricate network of base pairing and stacking interactions observed crystallographically[32] and by NMR[30] (Figure 4C, black bars). Specifically, reactivities in the binding pocket decreased (Figure 4A, regions J1-2 and J3-1), whereas reactivities increased at U62 and U63, consistent with the crystal structure that shows that these nucleotides are unpaired and likely highly dynamic in the ligand-bound state.[32] The reactivity of U48 increased 2-fold upon addition of 2AP [Figure 4A; $p < 0.04$; also consistent with the crystal structure of the ligand-bound RNA, which shows that this position is constrained in a conformation that facilitates SHAPE reactivity (Figure S7 of the Supporting Information)].[32,53]

Addition of 2AP to the aptamer *in vitro* also induced large conformational changes in the RNA (Figure 4B,C). The SHAPE profiles of the ligand-bound RNA in cells and in buffer with Mg^{2+} were similar (Figure S8 of the Supporting

dx.doi.org/10.1021/bi401207q | *Biochemistry* 2013, 52, 8777−8785

Information; also compare panels A and B of Figure 4). Because the starting structures of the RNA in cells and in buffer are different, the degree of conformational change induced by ligand binding in cells is different from (and generally smaller than) the degree of ligand-induced change in buffer (Figure 4C). In cells, there were only small changes in regions L2, J2-3, and J3-1 upon ligand binding. In buffer, the aptamer underwent substantial reactivity changes in these regions. In contrast, conformations of nucleotides in regions J1-2 and L3 changed more dramatically upon ligand binding in cells than in buffer. Overall, these observations indicate that the equilibrium between the free and bound aptamer states is different, and likely more favorable, in cells than in buffer.

We assessed the specificity of the conformational changes induced by 2AP with two additional ligands. 2,6-Diaminopurine binds the aptamer with high affinity ($K_D \approx 2$ nM).[55] As expected, this ligand also induced large changes in the in-cell aptamer SHAPE reactivity profile, and these changes were comparable to those induced by 2AP (Figure S9 of the Supporting Information). In contrast, N^6,N^6-dimethyladenine does not bind the aptamer ($K_D > 300$ μM),[26] and the in-cell SHAPE profile obtained from cells grown in the presence of this molecule was similar to that of the free aptamer (Figure S9 of the Supporting Information). These results emphasize that conformational changes induced by 2AP reflect specific binding in the ligand-binding pocket of the riboswitch.

Differences between In-Cell and Dilute Solution Structures Reflect Intrinsic Properties of the Riboswitch RNA. To confirm that differences between in-cell and *in vitro* SHAPE reactivity profiles of the free aptamer were not due to binding by endogenous adenine, we investigated a nonbinding mutant of the aptamer. U74 forms a canonical base pair with the adenine ligand that is critical for both ligand affinity and specificity.[26,54] We reasoned that a U74G mutation should disrupt binding to adenine, 2AP, and related molecules. The profiles of the U74G mutant in buffer at 1 mM Mg^{2+} in the absence and presence of 1 mM 2AP were essentially identical (Figure S10 of the Supporting Information), indicating that the mutant does not bind 2AP *in vitro*, even at high ligand concentrations.

In-cell analysis of the U74G mutant in the absence and presence of added 2AP also yielded nearly identical profiles (Figure 5A), indicating that the mutant does not bind ligand in cells. Critically, the nonbinding mutant exhibits differences between in-cell and *in vitro* states similar to those observed for the native sequence aptamer (Figure 5B,C). Thus, the nonbinding mutant and the native sequence aptamer adopt the same organized structure in cells, even in the absence of ligand. Therefore, the in-cell structure of the unliganded native sequence aptamer does not reflect binding by endogenous adenine. Instead, these data emphasize a critical role for the intracellular environment in governing the structure of this RNA.

High Mg^{2+} Concentrations Do Not Induce the Structure Observed in Cells. We attempted to induce the aptamer domain to adopt the in-cell conformation *in vitro* by increasing the added Mg^{2+} concentration. We probed the aptamer structure as a function of Mg^{2+} concentration and calculated the Pearson correlation coefficient (R) between in-cell and *in vitro* SHAPE reactivities (Figure 6). The correlation between the in-cell reactivities and those measured in buffer at 1 mM Mg^{2+} was low [0.55 (inset of Figure 6)], consistent with large differences in RNA structure under these two conditions.

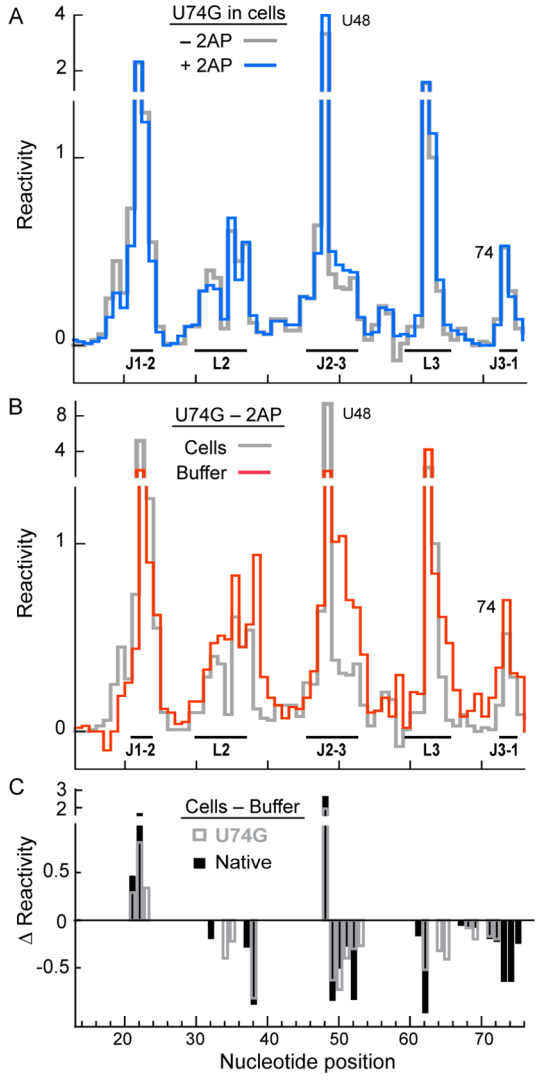

Figure 5. SHAPE reactivity profiles for the U74G nonbinding mutant (A) in the absence (gray) and presence (blue) of ligand in cells and (B) in the absence of ligand in cells (gray) and buffer (red). (C) Significant reactivity differences in cells compared to buffer with 1 mM Mg^{2+} for the wild type (solid black bars) and U74G mutant (empty gray bars) (two-tailed Student's t test; $p < 0.02$; $n = 3$).

At a Mg^{2+} concentration of 2 mM, the coefficient was 0.69. At 5 mM, the coefficient was 0.75, and no additional increase was observed up to the highest Mg^{2+} concentration tested, 30 mM. These data emphasize that, even in the presence of high Mg^{2+} concentrations, the ligand-free aptamer structure *in vitro* is different from that observed in cells. In summary, the conformation of the free aptamer RNA in cells features significantly more nucleotides whose conformations are similar to that of the fully folded ligand-bound state than to the structure that predominates under typical dilute solution conditions. Importantly, the in-cell state cannot be recapitulated in buffer by addition of a high concentration of Mg^{2+} ion.

DISCUSSION

The adenine riboswitch controls the expression of an adenosine deaminase gene in response to adenine levels. Like many noncoding RNAs, riboswitch function is mediated by the higher-order structure of the RNA. The crowded and unique ion environment in cells is likely to have a strong impact on

dx.doi.org/10.1021/bi401207q | *Biochemistry* 2013, 52, 8777–8785

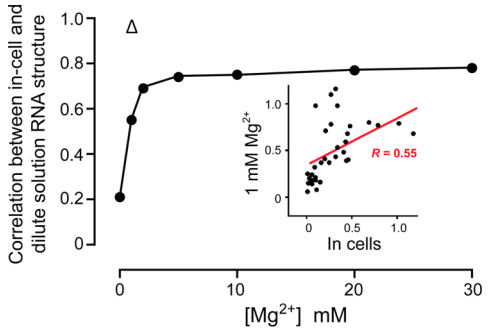

Figure 6. Correlation between in-cell and *in vitro* SHAPE reactivities for the ligand-free aptamer domain as a function of Mg^{2+} concentration. Data shown are from single-stranded and terminally base-paired nucleotides (A21-U25, U31-U39, A45-C54, G59-C67, and G72-U75) because these nucleotides show the largest structurally diagnostic changes. This correlation represents an upper limit. Inclusion of helix nucleotides, most of which have larger percent errors, results in an even poorer correlation (Figure S11 of the Supporting Information). The empty triangle represents the correlation between in-cell and *in vitro* reactivities for the ligand-bound aptamer domain in 1 mM Mg^{2+}. The inset shows *in vitro* reactivities at 1 mM Mg^{2+} plotted vs in-cell reactivities in the absence of ligand.

RNA structure–function relationships, but these effects remain largely unexplored. We probed the reactivities of individual nucleotides in the aptamer RNA with the SHAPE reagent, 1M7, which readily diffuses through the *E. coli* bacterium, modifies RNA *in vitro* and in cells with roughly equal probability, and measures RNA structure on a time scale of minutes. We found that the cellular environment induces a conformation in the unbound adenine riboswitch aptamer RNA that is different from both the unliganded structure *in vitro*, even in buffer at high Mg^{2+} concentrations, and the ligand-bound structure.

We visualized differences between structures of the adenine riboswitch aptamer domain in cells with other states examined here by superimposing statistically significant reactivity differences on the structure of the fully folded, ligand-bound RNA. For the in-cell, ligand-free RNA (Figure 7A), SHAPE reactivities suggest that long-range interactions between L2 and L3 are partially formed but that the J1-2 and J3-1 strands in the ligand-binding pocket are relatively unstructured (compare panels A and C of Figure 7). In buffer at 1 mM Mg^{2+}, nucleotides throughout the aptamer domain, including those in both the binding pocket and loop regions, are more reactive by SHAPE than in cells (Figure 7B, red regions). Nucleotides that form the L2–L3 tertiary interaction stabilize a collapsed form of the adenine aptamer that reduces the radius of gyration of the RNA by ~3 Å.[31] These data indicate that the RNA in healthy living cells is less reactive, likely more compact, and more highly structured than the purified RNA in buffer at 1 mM Mg^{2+} (Figure 7A,B).

In cells, the nonbinding U74G mutant has SHAPE reactivities virtually identical to those of the ligand-free, native sequence aptamer (Figure 5), emphasizing that the decrease in reactivity in cells does not arise from endogenous ligand binding. Addition of 2AP to the native sequence RNA in cells induced changes in SHAPE reactivity that fell largely in binding pocket (J1-2 and J3-1) regions (Figure 7C). The localized changes that differentiate the in-cell and plus-ligand states emphasize that much of the global RNA structure is at least partially stable in cells and that effects due to 2AP binding occur predominately in the ligand-binding pocket (compare panels A and C of Figure 7).

Strikingly, in buffer at 30 mM Mg^{2+}, SHAPE reactivities indicate that the aptamer domain structure is more similar to the structure in 1 mM Mg^{2+} than to the in-cell state (Figure 7D). Therefore, the cellular environment stabilizes the ligand-free aptamer to yield a higher-order structure that is not replicated by ligand binding or by high Mg^{2+} concentrations *in vitro*.

In summary, we examined the structure of the adenine riboswitch aptamer RNA in living cells at single-nucleotide resolution on a time scale of minutes using the fast-acting 1M7 SHAPE reagent. The intracellular environment induces a less SHAPE-reactive (and thus more highly conformationally constrained) conformation in the ligand-free aptamer, indicating that the unliganded RNA is significantly more structured in cells than *in vitro*. Widely used standard *in vitro* conditions, even

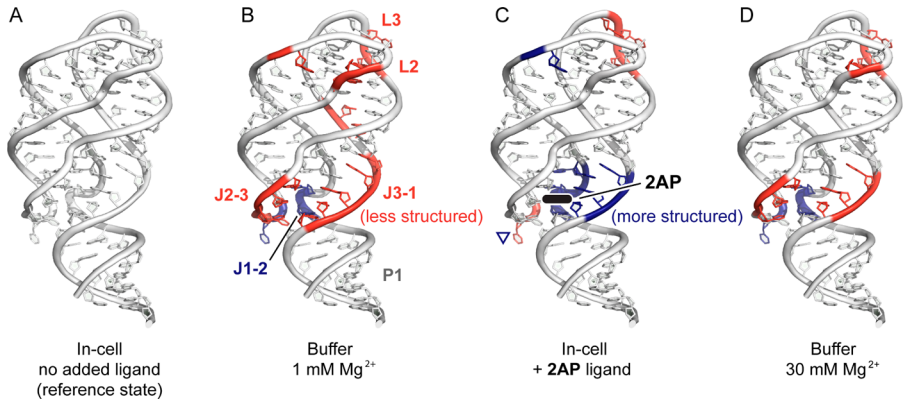

Figure 7. Nucleotide-resolution effects of the intracellular environment on adenine riboswitch aptamer domain RNA structure superimposed on the accepted ligand-bound structure (Protein Data Bank entry 1y26[32]). (A) The in-cell structure with no added ligand is defined as the reference state. Significant increases and decreases in nucleotide-resolution SHAPE reactivities relative to that of the in-cell RNA are colored red and blue, respectively. (B–D) Comparisons of the in-cell state with the aptamer RNA (B) in buffer at 1 mM Mg^{2+}, (C) in cells with added 2AP ligand, and (D) in buffer at 30 mM Mg^{2+}. The 2AP ligand, present in panel C, is colored black. The inverted blue triangle in panel C indicates that U48 is constrained in a hyper-reactive conformation (Figure S7 of the Supporting Information); thus, a higher (red) reactivity at this position reflects the increased (blue) level of structure in cells.

dx.doi.org/10.1021/bi401207q | *Biochemistry* 2013, 52, 8777–8785

at high Mg^{2+} concentrations, do not recapitulate the aptamer structure in cells. The complex cellular environment contains diverse small and large molecules that impose a combination of hard-core repulsions and repulsive and attractive chemical interactions on RNA.[9] Our observation that, in cells, the aptamer RNA is characterized by significantly more nucleotides whose conformations are similar to the fully folded ligand-bound state suggests that, overall, the in-cell environment exerts a strong net stabilizing effect on RNA structure. These differences in levels of RNA organization, readily detectable by SHAPE in-cell probing, are likely to have wide-ranging consequences for RNA structure and function.

■ ASSOCIATED CONTENT

Supporting Information

Figures S1−S11. This material is available free of charge via the Internet at http://pubs.acs.org.

■ AUTHOR INFORMATION

Corresponding Authors

*Address: 3258 Genome Sciences, University of North Carolina at Chapel Hill, Chapel Hill, NC 27699-3290. E-mail: weeks@unc.edu. Phone: (919) 962-7486.

*Address: 3250 Genome Sciences, University of North Carolina at Chapel Hill, Chapel Hill, NC 27699-3290. E-mail: gary_pielak@unc.edu. Phone: (919) 966-3671.

Funding

This work was supported by National Science Foundation Grants MCB-1051819 (to G.J.P.) and MCB-1121024 (to K.M.W.) and National Science Foundation Graduate Research Fellowship DGE-0646083 (to J.T.).

Notes

The authors declare no competing financial interests.

■ ACKNOWLEDGMENTS

We thank Luc Ponchon for guidance with the tRNA scaffold expression system, Oleg Favorov and Fethullah Karabiber for assistance in calculating the absolute amount of adduct formation *in vitro* and in cells, and Linda Spremulli for insightful discussions.

■ REFERENCES

(1) Zimmerman, S. B., and Trach, S. O. (1991) Estimation of macromolecule concentrations and excluded volume effects for the cytoplasm of *Escherichia coli*. *J. Mol. Biol. 222*, 599−620.

(2) Tabor, C. W., and Tabor, H. (1985) Polyamines in microorganisms. *Microbiol. Rev. 49*, 81−99.

(3) Miyamoto, S., Kashiwagi, K., Ito, K., Watanabe, S., and Igarashi, K. (1993) Estimation of polyamine distribution and polyamine stimulation of protein synthesis in *Escherichia coli*. *Arch. Biochem. Biophys. 300*, 63−68.

(4) Bennett, B. D., Kimball, E. H., Gao, M., Osterhout, R., Van Dien, S. J., and Rabinowitz, J. D. (2009) Absolute metabolite concentrations and implied enzyme active site occupancy in *Escherichia coli*. *Nat. Chem. Biol. 5*, 593−599.

(5) Wang, Y., Sarkar, M., Smith, A. E., Krois, A. S., and Pielak, G. J. (2012) Macromolecular crowding and protein stability. *J. Am. Chem. Soc. 134*, 16614−16618.

(6) Minton, A. P. (1981) Excluded volume as a determinant of macromolecular structure and reactivity. *Biopolymers 20*, 2093−2120.

(7) Zhou, H. X., Rivas, G., and Minton, A. P. (2008) Macromolecular crowding and confinement: Biochemical, biophysical, and potential physiological consequences. *Annu. Rev. Biophys. 37*, 375−397.

(8) Sarkar, M., Smith, A. E., and Pielak, G. J. (2013) Impact of reconstituted cytosol on protein stability. *Proc. Natl. Acad. Sci. U.S.A.*, DOI: 10.1073/pnas.1312678110.

(9) Sarkar, M., Li, C., and Pielak, G. J. (2013) Soft interactions and crowding. *Biophys. Rev. 5*, 187−194.

(10) Nakano, S., Karimata, H. T., Kitagawa, Y., and Sugimoto, N. (2009) Facilitation of RNA enzyme activity in the molecular crowding media of cosolutes. *J. Am. Chem. Soc. 131*, 16881−16888.

(11) Denesyuk, N. A., and Thirumalai, D. (2011) Crowding promotes the switch from hairpin to pseudoknot conformation in human telomerase RNA. *J. Am. Chem. Soc. 133*, 11858−11861.

(12) Kilburn, D., Roh, J. H., Guo, L., Briber, R. M., and Woodson, S. A. (2011) Molecular crowding stabilizes folded RNA structure by the excluded volume effect. *J. Am. Chem. Soc. 132*, 8690−8696.

(13) Draper, D. E. (2004) A guide to ions and RNA structure. *RNA 10*, 335−343.

(14) Trachman, R. J., III, and Draper, D. E. (2013) Comparison of interactions of diamine and Mg^{2+} with RNA rertiary structures: Similar versus differential effects on the stabilities of diverse RNA folds. *Biochemistry 52*, 5911−5919.

(15) Wells, S. E., Hughes, J. M., Igel, A. H., and Ares, M., Jr. (2000) Use of dimethyl sulfate to probe RNA structure *in vivo*. *Methods Enzymol. 318*, 479−493.

(16) Liebeg, A., and Waldsich, C. (2009) Probing RNA structure within living cells. *Methods Enzymol. 468*, 219−238.

(17) Wilkinson, K. A., Vasa, S. M., Deigan, K. E., Mortimer, S. A., Giddings, M. C., and Weeks, K. M. (2009) Influence of nucleotide identity on ribose 2′-hydroxyl reactivity in RNA. *RNA 15*, 1314−1321.

(18) Merino, E. J., Wilkinson, K. A., Coughlan, J. L., and Weeks, K. M. (2005) RNA structure analysis at single nucleotide resolution by selective 2′-hydroxyl acylation and primer extension (SHAPE). *J. Am. Chem. Soc. 127*, 4223−4231.

(19) Wang, B., Wilkinson, K. A., and Weeks, K. M. (2008) Complex ligand-induced conformational changes in tRNA(Asp) revealed by single-nucleotide resolution SHAPE chemistry. *Biochemistry 47*, 3454−3461.

(20) Weeks, K. M., and Mauger, D. M. (2011) Exploring RNA structural codes with SHAPE chemistry. *Acc. Chem. Res. 44*, 1280−1291.

(21) Grohman, J. K., Gorelick, R. J., Lickwar, C. R., Lieb, J. D., Bower, B. D., Znosko, B. M., and Weeks, K. M. (2013) A guanosine-centric mechanism for RNA chaperone function. *Science 340*, 190−195.

(22) Hajdin, C. E., Bellaousov, S., Huggins, W., Leonard, C. W., Mathews, D. H., and Weeks, K. M. (2013) Accurate SHAPE-directed RNA secondary structure modeling, including pseudoknots. *Proc. Natl. Acad. Sci. U.S.A. 110*, 5498−5503.

(23) Wilkinson, K. A., Gorelick, R. J., Vasa, S. M., Guex, N., Rein, A., Mathews, D. H., Giddings, M. C., and Weeks, K. M. (2008) High-Throughput SHAPE analysis reveals structures in HIV-1 genomic RNA strongly conserved across distinct biological states. *PLoS Biol. 6*, e96.

(24) Gherghe, C., Lombo, T., Leonard, C. W., Datta, S. A. K., Bess, J. W., Gorelick, R. J., Rein, A., and Weeks, K. M. (2010) Definition of a high-affinity Gag recognition structure mediating packaging of a retroviral RNA genome. *Proc. Natl. Acad. Sci. U.S.A. 107*, 19248−19253.

(25) Spitale, R. C., Crisalli, P., Flynn, R. A., Torre, E. A., Kool, E. T., and Chang, H. Y. (2013) RNA SHAPE analysis in living cells. *Nat. Chem. Biol. 9*, 18−20.

(26) Mandal, M., and Breaker, R. R. (2004) Gene regulation by riboswitches. *Nat. Rev. Mol. Cell Biol. 5*, 451−463.

(27) Lemay, J. F., Penedo, J. C., Tremblay, R., Lilley, D. M., and Lafontaine, D. A. (2006) Folding of the adenine riboswitch. *Chem. Biol. 13*, 857−868.

(28) Rieder, R., Lang, K., Graber, D., and Micura, R. (2007) Ligand-induced folding of the adenosine deaminase A-riboswitch and implications on riboswitch translational control. *ChemBioChem 8*, 896−902.

(29) Lin, J. C., and Thirumalai, D. (2008) Relative stability of helices determines the folding landscape of adenine riboswitch aptamers. *J. Am. Chem. Soc. 130*, 14080−14081.
(30) Lee, M. K., Gal, M., Frydman, L., and Varani, G. (2010) Real-time multidimensional NMR follows RNA folding with second resolution. *Proc. Natl. Acad. Sci. U.S.A. 107*, 9192−9197.
(31) Leipply, D., and Draper, D. E. (2011) Effects of Mg^{2+} on the free energy landscape for folding a purine riboswitch RNA. *Biochemistry 50*, 2790−2799.
(32) Serganov, A., Yuan, Y. R., Pikovskaya, O., Polonskaia, A., Malinina, L., Phan, A. T., Hobartner, C., Micura, R., Breaker, R. R., and Patel, D. J. (2004) Structural basis for discriminative regulation of gene expression by adenine- and guanine-sensing mRNAs. *Chem. Biol. 11*, 1729−1741.
(33) Froschauer, E. M., Kolisek, M., Dieterich, F., Schweigel, M., and Schweyen, R. J. (2004) Fluorescence measurements of free $[Mg^{2+}]$ by use of mag-fura 2 in *Salmonella enterica*. *FEMS Microbiol. Lett. 237*, 49−55.
(34) Grynkiewicz, G., Poenie, M., and Tsien, R. Y. (1985) A new generation of Ca^{2+} indicators with greatly improved fluorescence properties. *J. Biol. Chem. 260*, 3440−3450.
(35) Ponchon, L., and Dardel, F. (2007) Recombinant RNA technology: The tRNA scaffold. *Nat. Methods 4*, 571−576.
(36) Ponchon, L., Beauvais, G., Nonin-Lecomte, S., and Dardel, F. (2009) A generic protocol for the expression and purification of recombinant RNA in *Escherichia coli* using a tRNA scaffold. *Nat. Protoc. 4*, 947−959.
(37) Deigan, K. E., Li, T. W., Mathews, D. H., and Weeks, K. M. (2009) Accurate SHAPE-directed RNA structure determination. *Proc. Natl. Acad. Sci. U.S.A. 106*, 97−102.
(38) Cayley, S., Lewis, B. A., Guttman, H. J., and Record, M. T., Jr. (1991) Characterization of the cytoplasm of *Escherichia coli* K-12 as a function of external osmolarity. Implications for protein-DNA interactions *in vivo*. *J. Mol. Biol. 222*, 281−300.
(39) Karabiber, F., McGinnis, J. L., Favorov, O. V., and Weeks, K. M. (2013) QuShape: Rapid, accurate, and best-practices quantification of nucleic acid probing information, resolved by capillary electrophoresis. *RNA 19*, 63−73.
(40) Wee, S., and Wilkinson, B. J. (1988) Insights into the cell envelope of *Paracoccus denitrificans*, a member of the α-subdivision of purple bacteria, through studies of its lysozyme susceptibility. *Can. J. Microbiol. 34*, 952−959.
(41) London, R. E. (1991) Methods for measurement of intracellular magnesium: NMR and fluorescence. *Annu. Rev. Physiol. 53*, 241−258.
(42) Hurley, T. W., Ryan, M. P., and Brinck, R. W. (1992) Changes of cytosolic Ca^{2+} interfere with measurements of cytosolic Mg^{2+} using mag-fura-2. *Am. J. Physiol. 263*, C300−C307.
(43) Tashiro, M., and Konishi, M. (1997) Basal intracellular free Mg^{2+} concentration in smooth muscle cells of guinea pig tenia cecum: Intracellular calibration of the fluorescent indicator furaptra. *Biophys. J. 73*, 3358−3370.
(44) Mortimer, S. A., and Weeks, K. M. (2007) A fast-acting reagent for accurate analysis of RNA secondary and tertiary structure by SHAPE chemistry. *J. Am. Chem. Soc. 129*, 4144−4145.
(45) Mastro, A. M., Babich, M. A., Taylor, W. D., and Keith, A. D. (1984) Diffusion of a small molecule in the cytoplasm of mammalian cells. *Proc. Natl. Acad. Sci. U.S.A. 81*, 3414−3418.
(46) Safranyos, R. G., and Caveney, S. (1985) Rates of diffusion of fluorescent molecules via cell-to-cell membrane channels in a developing tissue. *J. Cell Biol. 100*, 736−747.
(47) Jasnin, M., Moulin, M., Haertlein, M., Zaccai, G., and Tehei, M. (2008) Down to atomic-scale intracellular water dynamics. *EMBO Rep. 9*, 543−547.
(48) Mika, J. T., Van Den Bogaart, G., Veenhoff, L., Krasnikov, V., and Poolman, B. (2010) Molecular sieving properties of the cytoplasm of *Escherichia coli* and consequences of osmotic stress. *Mol. Microbiol. 77*, 200−207.
(49) Mika, J. T., and Poolman, B. (2011) Macromolecule diffusion and confinement in prokaryotic cells. *Curr. Opin. Biotechnol. 22*, 117−126.
(50) Gherghe, C. M., Mortimer, S. A., Krahn, J. M., Thompson, N. L., and Weeks, K. M. (2008) Slow conformational dynamics at C2′-endo nucleotides in RNA. *J. Am. Chem. Soc. 130*, 8884−8885.
(51) Mortimer, S. A., and Weeks, K. M. (2009) C2′-endo nucleotides as molecular timers suggested by the folding of an RNA domain. *Proc. Natl. Acad. Sci. U.S.A. 106*, 15622−15627.
(52) Steen, K. A., Rice, G. M., and Weeks, K. M. (2012) Fingerprinting noncanonical and tertiary RNA structures by differential SHAPE reactivity. *J. Am. Chem. Soc. 134*, 13160−13163.
(53) McGinnis, J. L., Dunkle, J. A., Cate, J. H., and Weeks, K. M. (2012) The mechanisms of RNA SHAPE chemistry. *J. Am. Chem. Soc. 134*, 6617−6624.
(54) Lemay, J. F., and Lafontaine, D. A. (2007) Core requirements of the adenine riboswitch aptamer for ligand binding. *RNA 13*, 339−350.
(55) Dixon, N., Duncan, J. N., Geerlings, T., Dunstan, M. S., McCarthy, J. E., Leys, D., and Micklefield, J. (2010) Reengineering orthogonally selective riboswitches. *Proc. Natl. Acad. Sci. U.S.A. 107*, 2830−2835.

Supporting Information for:

The Cellular Environment Stabilizes Adenine Riboswitch RNA Structure

Jillian Tyrrell, Jennifer L. McGinnis, Kevin M. Weeks*, Gary J. Pielak*

* Correspondence: gary_pielak@unc.edu and weeks@unc.edu

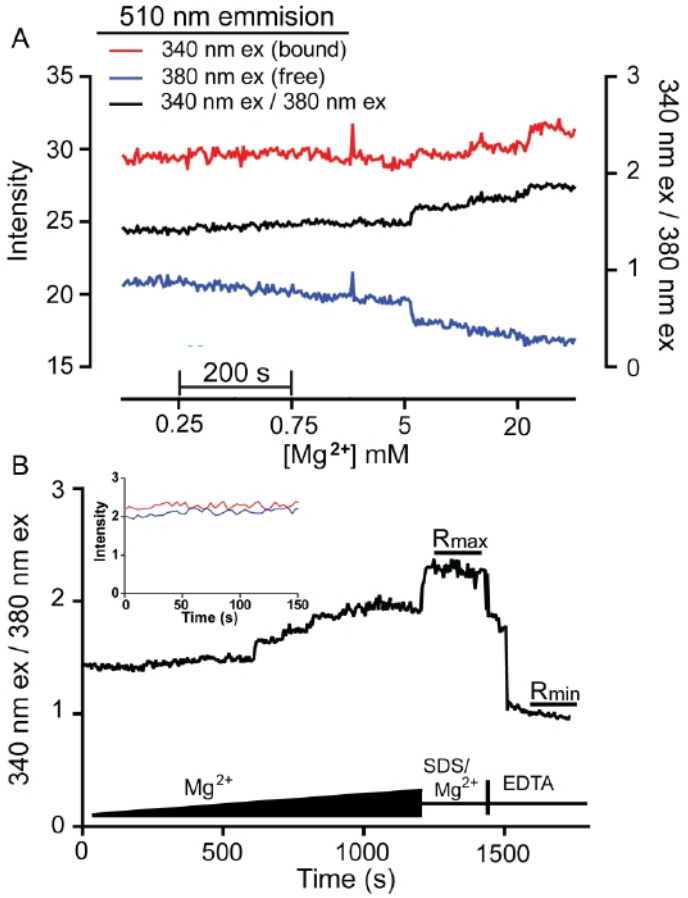

Figure S1. Free intracellular Mg^{2+} concentration in *E. coli* cells measured ratiometrically using mag-fura-2 is < 1 mM. **(A)** Single wavelength fluorescence intensities at 510 nm with excitation at 340 nm (red) and 380 nm (blue), corresponding to the bound and free dye, respectively, were measured as a function of added Mg^{2+}. The ratios (black) are used in Eqn. 1 to obtain the concentration of free Mg^{2+} in cells. **(B)** Ratio of 510 nm emission intensities from 340 nm and 380 nm excitation for a complete Mg^{2+}-measurement experiment. Initial portion of the ratio plot (black) is the Mg^{2+} titration shown in panel A. R_{max} was measured by adding SDS (0.1% m/v final concentration) and additional Mg^{2+} (30 mM final concentration) to the cells. R_{min} was measured by adding excess EDTA to chelate the Mg^{2+}. R_{min} and R_{max} were consistent across all experiments (R_{max} = 2.02 ± 0.20, R_{min} = 0.95 ± 0.05).

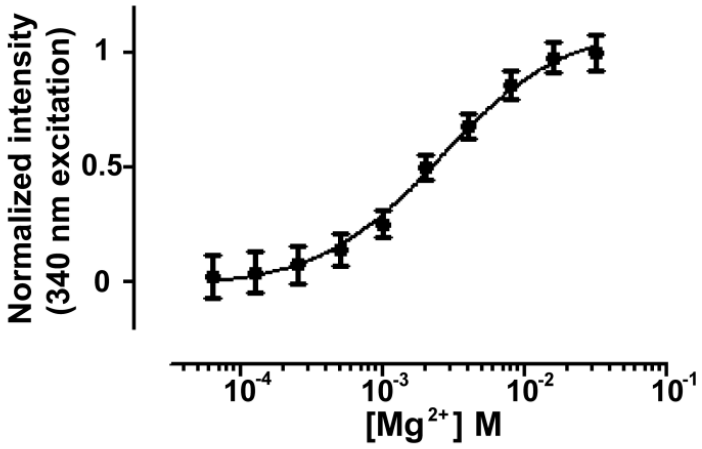

Figure S2. Determination of the K_D of the mag-fura-2–Mg^{2+} complex. Normalized intensities at 510 nm (340 nm excitation) were measured in a physiological-like buffer (see Methods) as a function of Mg^{2+} concentration. Intensities were fit to a single-site binding equation to yield the transition midpoint, corresponding to a K_D of 2.5 mM.

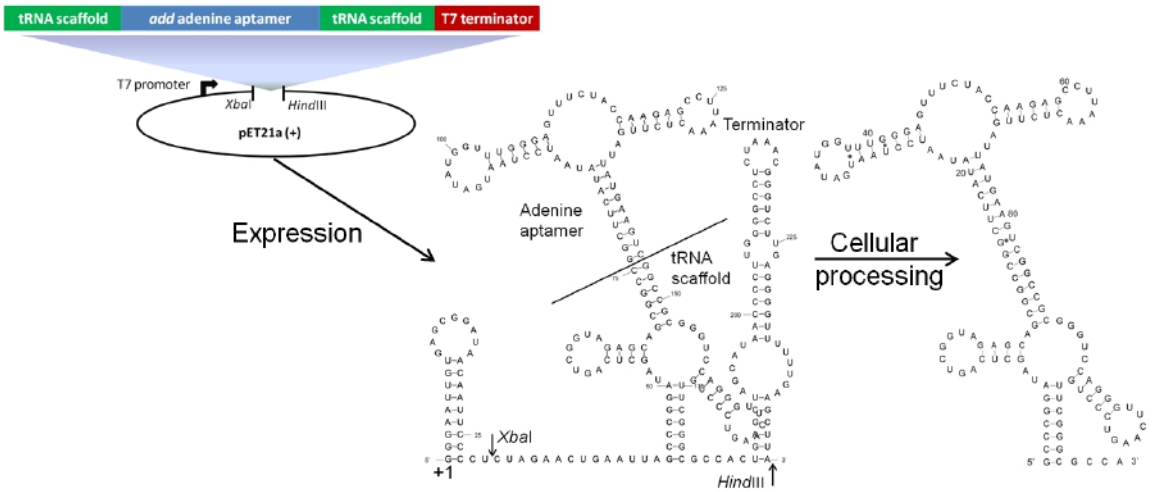

Figure S3. Chimeric tRNA-aptamer domain vector design and expression.

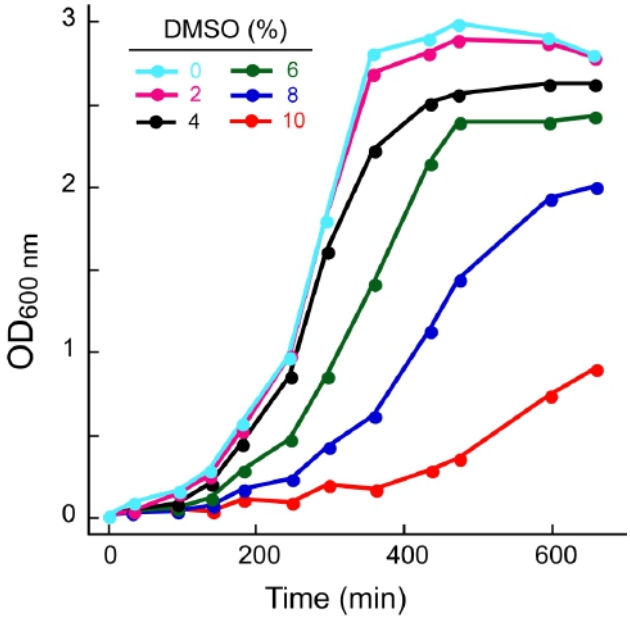

Figure S4. Effect of DMSO on *E. coli* growth rate. DMSO concentrations below 4% (v/v) do not significantly perturb cell viability. A final DMSO concentration of 2% (v/v) was used for in-cell SHAPE in this work. DH5α cells (500 mL) were grown in LB to an OD_{600} of 0.3 starting from 5 mL of an overnight culture. Cell aliquots (10 mL) were then added to 90 mL of LB containing 0–10% (v/v) DMSO. Samples were withdrawn at intervals, and the OD_{600} was measured to assess cell growth. The resulting growth curves show that *E. coli* cells are fully viable at DMSO concentrations below 4% (vol/vol) but growth is compromised at 10% co-solvent.

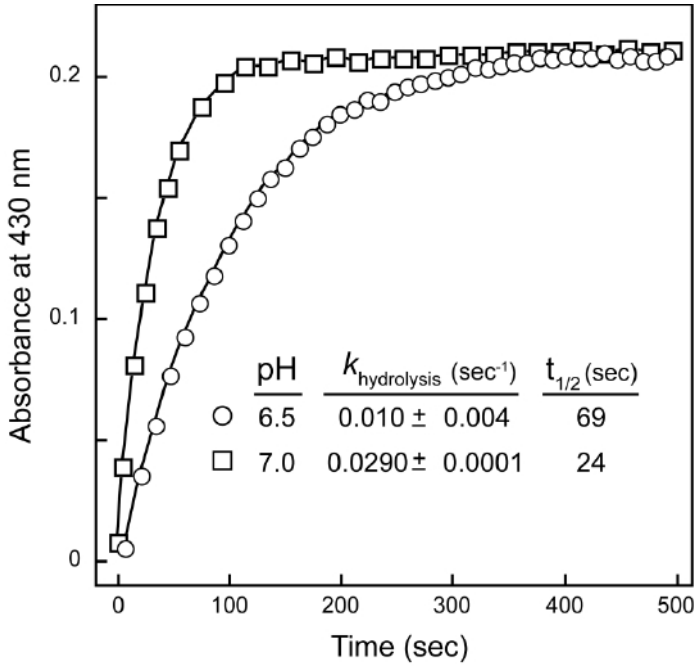

Figure S5. Pseudo-first order hydrolysis of 1M7 in LB at 37 °C at pH values of 6.5 and 7.0, which correspond to that of the culture media at the beginning and in the late-log phases of cell growth. Reagent hydrolysis was measured in a cuvette at 37 °C by adding 100 μL of 2.0 mM 1M7 in DMSO to 900 μL of equilibrated LB (pH 6.5 or 7.0). Pseudo-first-order rate constants were obtained by monitoring the 430 nm absorbance of the hydrolysis product (2-methylamino-4-nitrobenzoate).

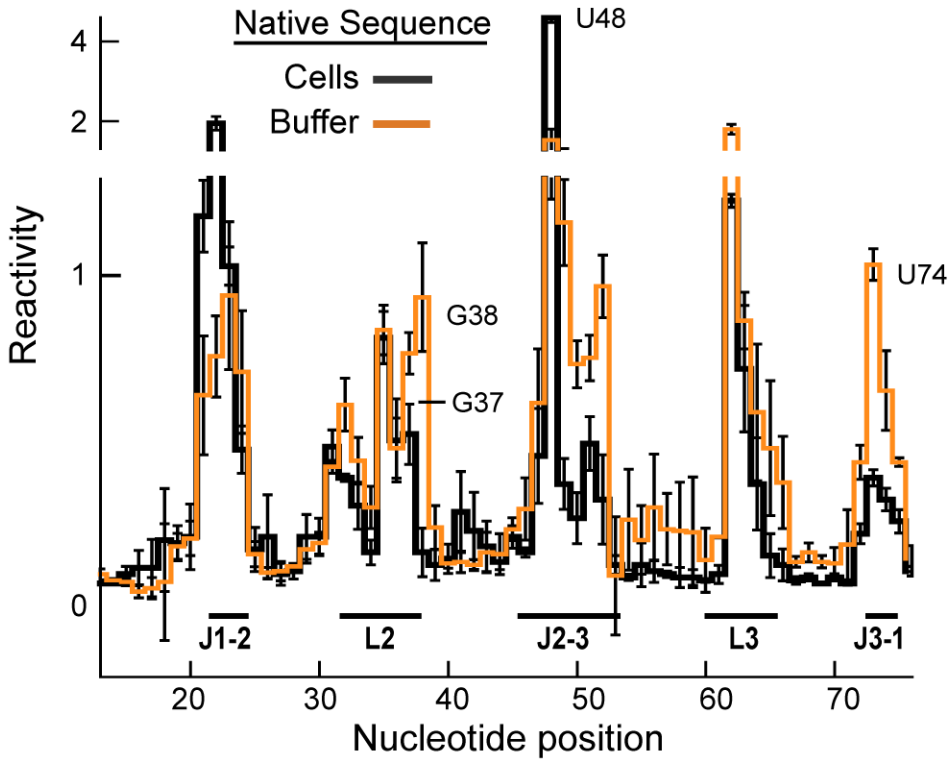

Figure S6. In-cell SHAPE. Processed SHAPE reactivity profiles from Figure 3 for the adenine aptamer domain in cells (black) and in buffer at 1 mM Mg^{2+} (orange), with additional error information. Error bars represent the standard error from the mean from 3 experiments.

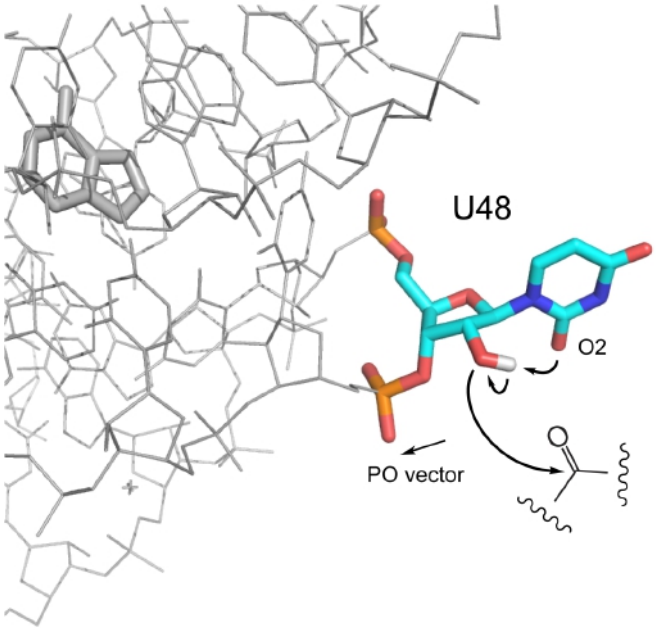

Figure S7. Mechanism of SHAPE hyper-reactivity at nucleotide U48. The conformation encompasses two features that facilitate SHAPE reactivity. First, the anionic 3'-phosphate diester is directed away from the reactive 2'-hydroxyl group (illustrated as the PO vector). Second, the 2-keto group of the uracil moiety is positioned to function as a general base and lower the pK_a of the attacking 2'-OH group.

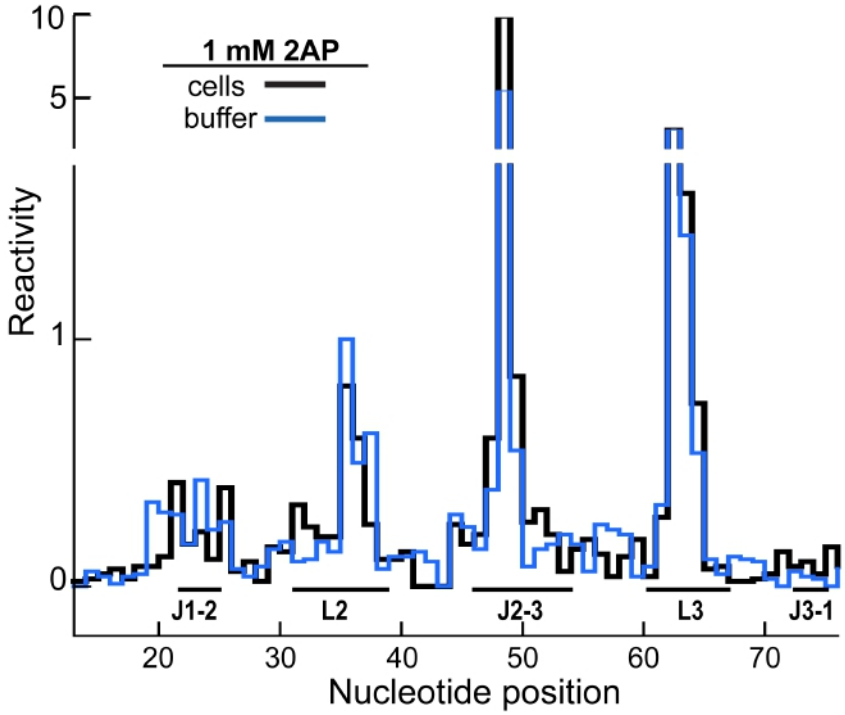

Figure S8. Reactivity profiles of the 2AP-bound aptamer *in vitro* (blue) and in cells (black). 2AP (1 mM) was added to purified aptamer *in vitro* or cell media. These data are the same as shown in Figure 4 panels A and B, but are superimposed here for additional clarity.

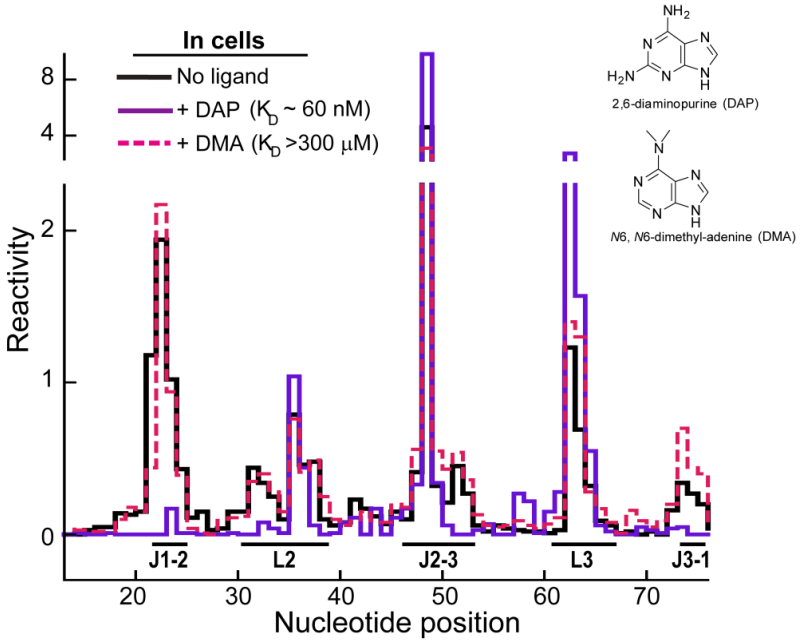

Figure S9. In cells, the aptamer binds 2,6-diaminopurine (DAP) but not *N*6,*N*6-dimethyl-adenine (DMA). SHAPE reactivity in cells without ligand and with 1 mM DAP or DMA. The y-axis values at the top indicate reactivities at position U48.

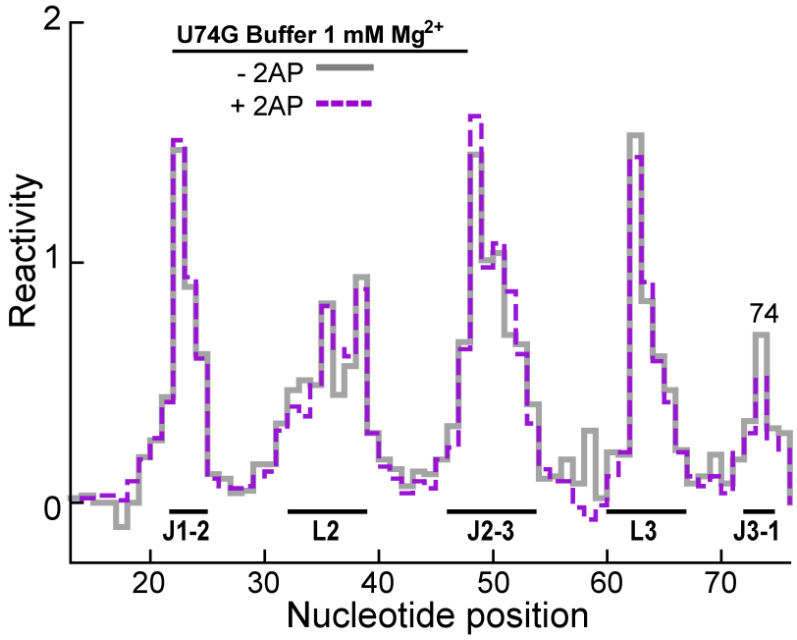

Figure S10. U74G mutant does not bind ligand *in vitro*. SHAPE reactivities for the native sequence aptamer and the U74G mutant in the presence and absence of 2AP at a final concentration of 1 mM ligand.

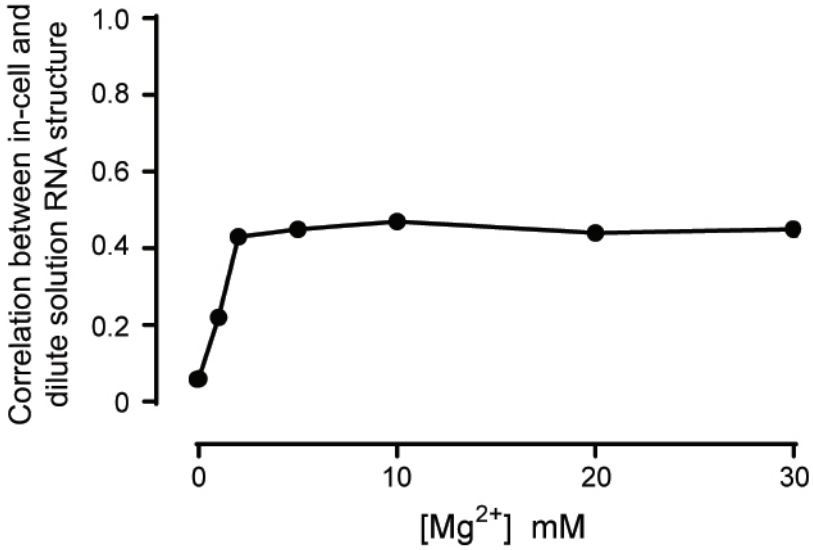

Figure S11. Correlation between in-cell and *in vitro* SHAPE reactivities for the ligand-free aptamer domain RNA as a function of Mg^{2+} concentration. Data include all nucleotides.